

Coupling between vortices and antivortices in a cross-tie wall studied by time-resolved SEMPAFabian Klodt-Twesten,^{1,*} Susanne Kuhrau,¹ Philipp Staeck,¹ Demetrio R. Cavicchia,^{1,†}
Fabian Lofink,^{1,2} Hans Peter Oepen,¹ and Robert Frömter¹¹*Universität Hamburg, Center for Hybrid Nanostructures, Luruper Chaussee 149, 22761 Hamburg, Germany*²*Fraunhofer Institute for Silicon Technology, Fraunhoferstrasse 1, 25524 Itzehoe, Germany*

(Received 27 October 2017; published 23 January 2018)

Using time-resolved scanning electron microscopy with polarization analysis (TR-SEMPA) the dynamics of magnetic vortices and antivortices in a cross-tie wall is investigated. Under quasistatic external field drive both quasiparticles oscillate at opposite phase to each other (in analogy to an optical mode). An additional common motion, which stems from the finite boundary conditions in a patterned FeCoSiB rectangle, is observed (in analogy to an acoustic mode), leading in total to a stronger field-dependent displacement for the vortices compared to the antivortices. Both types of magnetic solitons are mutually coupled via the minimization of the total magnetic energy of the structure. It is shown that the TR-SEMPA results can be explained via coupling in the framework of micromagnetic simulations and that the coupling constants can be extracted. The motion is composed from the contributions of the two terminating vortices and a mutual vortex-antivortex coupling along the chain.

DOI: [10.1103/PhysRevB.97.024426](https://doi.org/10.1103/PhysRevB.97.024426)**I. INTRODUCTION**

Vortices and antivortices are topological objects that are found in thin films of soft magnetic materials. The stray-field energy of the nanostructure is reduced by a curling of the in-plane magnetization around the center of the soliton [1]. In the center of the curling magnetization, however, the exchange will create a very large energy contribution that cannot be balanced by the gain of the stray-field energy. The structure that gives the minimum of total energy is a continuous tilting of magnetization out of the plane in a very small area with radius of a few nanometers, the so-called core [2–6]. Due to the high stability of these spin configurations under current and magnetic-field excitations, they can be treated in the framework of the Thiele model [7] as quasiparticles and can be classified according to their winding number $n = \frac{1}{2\pi} \oint \vec{\nabla} \varphi \cdot d\vec{s}$, where φ is the in-plane magnetization angle. The topological winding number is $n = 1$ (-1) for vortices (antivortices) indicating the different magnetization rotation around the core.

Several studies have been performed on the dynamics of individual vortices [8–16], which form as the magnetic ground state in nanostructured disks and rectangles of certain dimensions. On the contrary, investigating the dynamics of individual antivortices requires more complex nanostructures to stabilize the antivortex [17,18]. A displacement of the core of individual (anti-)vortices out of the equilibrium position results in a distortion of adjacent in-plane domains, increasing stray-field and exchange energy [15,19–21]. For moderate displacements this leads to a linear restoring force, i.e., a harmonic confining potential for the quasiparticles [22]. A similar situation occurs when two magnetic solitons approach each other. As

a function of the distance between the solitons, the stray-field and exchange energies of the in-plane magnetized area change, which results in a coupling of the quasiparticles. Due to the very narrow size of the out-of-plane magnetized core regions, the direct stray-field coupling between the cores can be neglected at reasonable separations. Hence, the effective coupling is independent of core polarity in the quasistatic case. For gyrotropic motion, however, the polarity determines the sense of core gyration for vortices and antivortices and the dynamical coupling will be influenced by polarity. Accordingly, the stray-field and exchange energies of the surrounding in-plane magnetization configuration are important for the coupling potential. In a very recent paper, Eggebrecht *et al.* [23] mapped out the radial pair-correlation function between vortices and antivortices as well as between two vortices in a network of metastable vortex-antivortex configurations in an extended iron film, finding different behaviors for the different pairs. Coupling between two vortices in a single nanostructure has been intensively studied, both theoretically [24–26] and experimentally [27,28]. However, there are no present studies on the coupling between vortices and antivortices, neither experimentally nor theoretically. Here, we investigate the coupling in a vortex-antivortex chain, also known as a cross-tie wall [3], that is confined in a nanostructure. A first observation of the dynamics in a comparable system has been published by Miguel *et al.* [29].

We record the magnetization dynamics via time-resolved scanning electron microscopy with polarization analysis (TR-SEMPA) [30]. This technique is based on a scanning electron microscope with polarization analysis (SEMPA) [31–33] that detects the spin polarization of secondary electrons via spin-polarized low-energy electron diffraction using single-electron counting [34]. The spin polarization of secondary electrons is a vectorial quantity that is directly related to the local magnetization vector at the sample surface. After scattering the electrons at a W(001) surface, two components of the spin polarization become accessible as mutual intensity asymmetries of the four (2,0) beams [32,35,36]. Thus, we are able to image both

* Author to whom correspondence should be addressed:

fabian.klodt@physik.uni-hamburg.de

† Present address: GLP Intellectual Property Office, Viale Europa Unita 171, 33100 Udine, Italy.

in-plane components of the magnetization simultaneously, which is advantageous for resolving cross-tie walls as recently demonstrated by Lofink *et al.* in a static experiment [37]. Furthermore, SEMPA, with a resolution down to 3 nm [38], has proven as a successful tool to resolve small magnetic objects like domain walls between out-of-plane domains [39–41].

The concept of time-resolved SEMPA makes use of the fact that the spin detector in SEMPA works in single-electron counting mode. Each secondary electron diffracted into one of the four (2,0) low-energy electron diffraction beams is amplified by a multichannel-plate assembly into a voltage pulse that can be electronically processed. In static SEMPA only the time-integrated count rate of the four channels is used to determine the local magnetization. Assuming fixed transit times for all electrons through the detector, the arrival time of each pulse in addition carries the information on the magnetic state a fixed time difference earlier. Thus, by recording the arrival time (phase) of each voltage pulse with respect to a periodic external drive, the whole asymmetry dataset can be sliced into fixed time intervals, yielding a movie of the time-resolved magnetization. In contrast to state-of-the-art stroboscopic approaches such as scanning transmission x-ray [42] or Lorentz microscopy [43], the primary electron beam is continuously on in TR-SEMPA and only the *ex situ* detection scheme is modified. In this way, a temporal resolution of 700 ps was demonstrated with our setup by Frömter *et al.* in 2016 [30].

II. EXPERIMENT

The sample consists of 40-nm-thick squares and rectangles structured from a sputtered $\text{Fe}_{70}\text{Co}_8\text{Si}_{12}\text{B}_{10}$ film on top of a gold microstrip (6.4- μm width; sputtered 60-nm gold on 24-nm chromium seed layer) on a sapphire substrate. The amorphous FeCoSiB film, while having a low magnetic anisotropy as Permalloy, shows a much stronger image contrast in SEMPA, which is due to the higher spin polarization of iron compared to nickel in the valence band [36]. Further details about the sample preparation can be found elsewhere [30]. An SEM micrograph of the whole strip is shown in the topmost panel of Fig. 1. Below, the in-plane components of the magnetization along the y and x directions are displayed. All magnetic rectangles are either in the diamond state, containing 2 vortices, or in a cross-tie state, containing $2+x$ vortices and x antivortices with $x=3,4$ (Fig. 1). We focused on a magnetic structure containing five vortices separated by four antivortices. This structure is framed with a dashed line and a zoom shown on the bottom-right side of Fig. 1. The vortices and antivortices are confined in a $1.5\text{-}\mu\text{m} \times 3.8\text{-}\mu\text{m} \times 40\text{-nm}$ FeCoSiB structure. In the lower-left part of Fig. 1, the sample geometry is sketched. The sketch shows the direction of the applied ac current through the microstrip, which generates an Oersted field along the y direction to drive the magnetization of the FeCoSiB structures. The time-dependent displacements of the (anti-)vortices along the x direction are plotted in Fig. 2(a). Individual (anti-)vortex positions have been fitted in eight TR-SEMPA images at different delays. One of the eight images is shown in Fig. 2(b). While the vortices (red squares and circles) exhibit a clear oscillation, the antivortices (blue diamonds and triangles) show a much smaller amplitude, but with identical phase. In addition

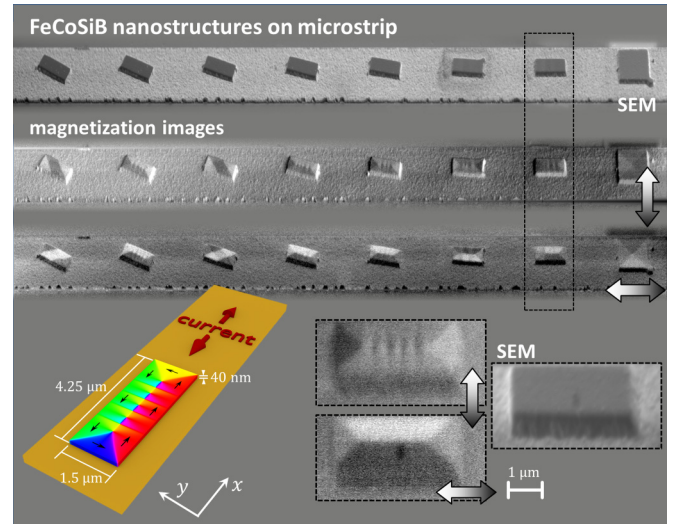


FIG. 1. Sample geometry and magnetic state of the FeCoSiB rectangles on a Au/Cr microstrip. The topography and magnetization of several individual rectangles are shown. The micrographs of the marked structure (both components of the in-plane magnetization and an SEM image) are displayed on the bottom-right side. As visible in the vertical magnetization component, four cross-tie develop in the structure. A schematic of the sample geometry is shown on the lower-left side. An electrical current in the positive x direction (technical) results in a magnetic field pointing in the negative y direction above the microstrip.

to a common oscillation of all solitons (analog to an acoustic mode), the different quasiparticles oscillate at opposite phase to each other (analog to an optical mode) so that the remaining antivortex motion is small.

Exciting the nanostructure close to resonance (via simulation we estimate for the anticyclic gyration with synchronous y motion for vortices and antivortices a resonance frequency around 130 MHz), gyration terms will become important, which makes a disentanglement between gyration, damping, and coupling effects necessary [44]. To avoid this complexity, the measurement is performed under quasistatic excitation, as the excitation frequency of 1 MHz is small compared to the resonance frequency. Thus, we can assume that the magnetization is in a quasiequilibrium state (field dependent) and that the intrinsic time evolution of the magnetization plays no role. This is consistent with the absence of gyration, as we observe no time-dependent y position of either vortices or antivortices. The (anti-)vortex displacement depends solely on the strength of the driving magnetic field. The plot in Fig. 2(c) gives the linear relation of quasiparticle displacement and magnetic-field strength. The strength of the magnetic field has been calculated from the current in the microstrip [45]. The phase of the magnetic response and the field are assumed to be identical as the dynamics are quasistatic. To verify phase and amplitude of the driving field the vortex displacement in a neighboring FeCoSiB square ($3.6\text{ }\mu\text{m} \times 3.6\text{ }\mu\text{m} \times 40\text{ nm}$), which contains a Landau state [SEMPA image shown as inset in Fig. 2(d)] is recorded. As the distance between the rectangular structure and the square is about $10\text{ }\mu\text{m}$ (see Fig. 1) a theoretical phase shift of 50 fs has to be expected, which is nonresolvable in our experiment. Micromagnetic simulations allow one to model the

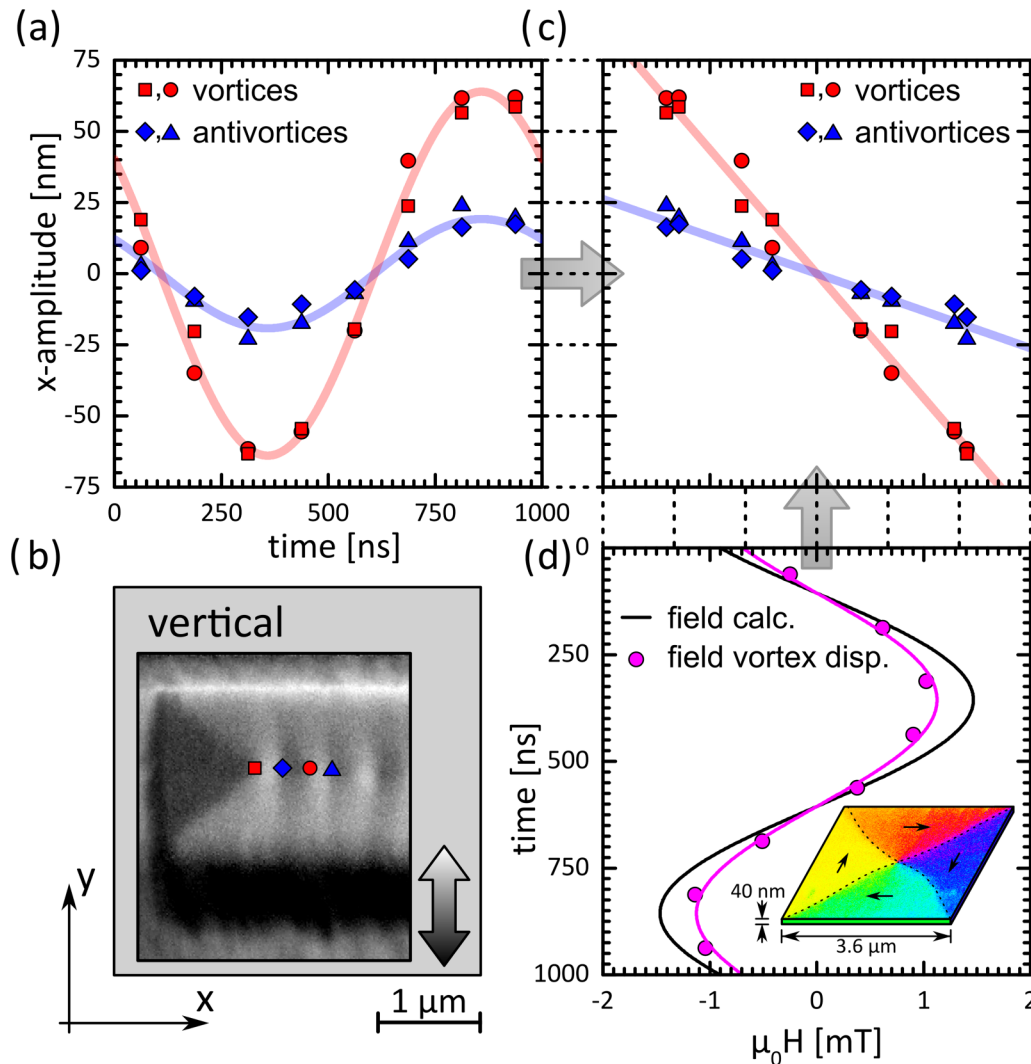


FIG. 2. Coupled vortex-antivortex oscillation, imaged with TR-SEMPE. Panel (b) shows one 125-ns-long snapshot of the vertical magnetization component from a TR-SEMPE movie of the microstructure shown in Fig. 1. From line profiles the (anti-)vortex displacement in the x direction as a function of time is obtained in panel (a). As no (anti-)vortex shift in the y direction could be detected, the excitation frequency is far below the resonance frequency and the solitons follow the magnetic excitation quasistatically. Panel (d) displays the magnetic field as a function of time, calculated from the measured microstrip peak-current amplitude of 15 mA (black curve). In the inset, the SEMPE micrograph of a FeCoSiB square in the Landau state is shown that has been measured in parallel. Comparing the observed vortex displacement in this structure with simulations confirms the calculated magnetic field strength (pink points and curve). Panel (c) combines the information from panels (a) (soliton displacement) and (d) (magnetic field). Both types of solitons follow a linear behavior with different but negative slopes under the external field.

observed vortex oscillation in the Landau pattern, which yields an independent determination of the magnetic field. The latter values are plotted as pink circles in Fig. 2(d). The pink and black curves roughly indicate the same magnitude for the driving magnetic field. The difference is probably due to slight deviations of the geometry and material parameters entering the simulation (thickness 40 nm; exchange stiffness 20 pJ/m [46]; saturation magnetization 1200 kA/m [47]). For this reason, we use the black curve as measure of the magnetic field in Fig. 2(c).

In the following, we will discuss the (anti-)vortex displacements shown in Fig. 2(c). Both vortices and antivortices show a linear dependence on the driving magnetic field. Although they move in the same direction, they have different slopes. The low driving frequency ensures that dynamic effects (gyration,

damping) can be neglected and that the quasiequilibrium state (field dependent) of the microstructure is observed. Especially the influence of pinning as a damping mechanism, which is a localized, nonlinear behavior, can be ruled out because of the excellent linearity of (anti-)vortex displacement on field. For these reasons, the different slopes cannot be explained as an effect of damping affecting both types of quasiparticles differently, and we conclude that another effect is responsible for this behavior. A qualitatively similar observation was made on a different microstructure of the same sample containing only three instead of four antivortices. Such a behavior has been previously reported in an x-ray photoelectron emission microscope investigation with pulsed excitation on Permalloy microstructures of different dimensions [29]. The authors

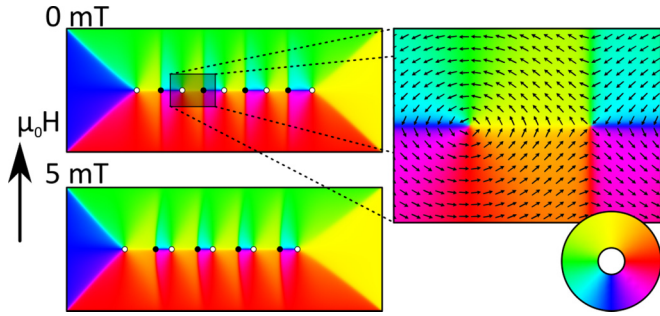


FIG. 3. Simulated equilibrium states of the cross-tie microstructure under the action of an external field of 0 and 5 mT. The magnetization is color coded with respect to the color wheel at the bottom right. A magnified image of the marked area is shown on the right side, where arrows indicate the direction of magnetization.

state that “the antivortices seem to be insensitive to the magnetic pulse.” As previously pointed out we are able to exclude any effect of gyration or damping from the different configurations due to the quasistatic excitation. In the field-dependent equilibrium state there is a balance between a deflecting force (from the Zeeman energy) and a restoring force (from the discussed coupling potential). We will therefore, in the following, investigate this balance with micromagnetic simulations and compare the results with our experiment.

III. SIMULATION

Micromagnetic simulations are performed using MICRO-MAGNUM [48] with a cell size of $5 \times 5 \times 40 \text{ nm}^3$ to understand the experimentally observed quasiparticle displacement. While anisotropies are neglected, an exchange stiffness of 20 pJ/m and a saturation magnetization of 1200 kA/m [47] are used to describe the (anti-)vortex displacement under the action of an external field. Simulated equilibrium states of the microstructure in an external field of 0 and 5 mT are shown in Fig. 3. The magnetization is color coded according to the color wheel in the bottom-right side (blue: magnetization points down, red: magnetization points to the right, etc.). An oppositely oriented displacement of both types of quasiparticles is expected, as the Zeeman energy prefers an alignment of the magnetization parallel to the external field and domains oriented parallel to the field (yellow) should grow, while domains oriented antiparallel (blue) should shrink. The exchange- and stray-field energies create a coupling potential, which counteracts these growths and shrinks and yields a field-dependent equilibrium distance of both solitons. One expects an oppositely directed displacement of antivortices and vortices. The field in the $+y$ -direction will drive the vortex to the left ($-x$ direction) and the antivortex to the right ($+x$ direction). However, the closure domains between microstructure border and vortex are much larger than the domains between vortex and antivortex. These domains lead under the action of an external field ($+y$ direction) to a shift of the whole vortex-antivortex-chain to the left ($-x$ direction). It is reasonable that both effects add up to the net (anti-)vortex displacement seen in Fig. 2(c).

Figure 4(a) shows the positions of both kinds of quasiparticles as a function of the external field (vortices red marks,

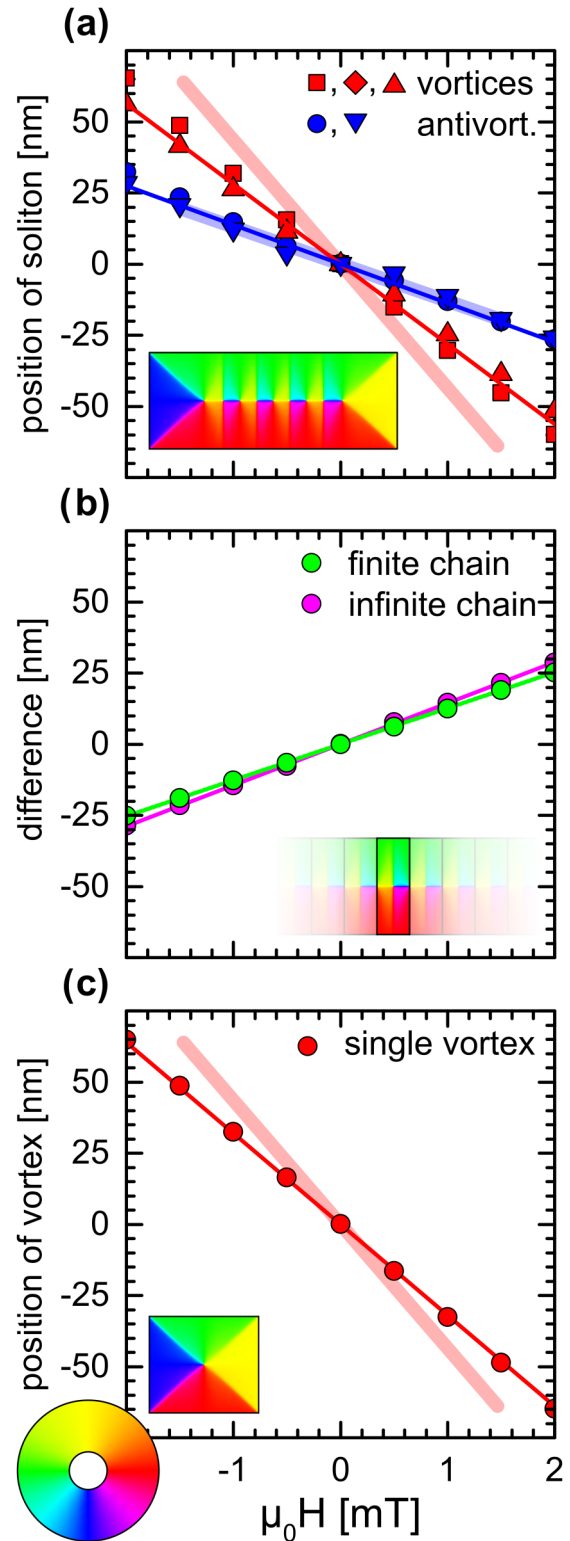


FIG. 4. Simulation of coupled vortex-antivortex oscillation. Panel (a) compares simulation results and experimentally obtained (anti-)vortex displacement for the rectangular FeCoSiB structure. A further outcome is that the observed oscillation of both solitons can be decomposed in a relative vortex-antivortex-oscillation with periodic boundary conditions (b) and a common-mode contribution from the absolute vortex displacement in a close-to-square rectangle (c).

antivortices blue). The simulated structure is shown in the inset and color coded with respect to the color wheel on the bottom left of Fig. 4. As observed in the experiment, both vortices and antivortices move in the same direction but with different slopes. The shaded areas in the background indicate the range of experimental data from Fig. 2(c). Small deviations from the experiment can be ascribed to deviations in the parameters used for simulation. Simulation as well as experiment gives larger displacements for the vortices compared to the antivortices. Therefore, the distance between both varies, which addresses the coupling between the quasiparticles. This oppositely directed displacement is superimposed onto a common displacement of all quasiparticles. Simulations show that both contributions can be decomposed into a vortex-antivortex chain with periodic boundary conditions, as shown in Fig. 4(b), and into a single vortex in a rectangular microstructure, as shown in Fig. 4(c). Using periodic boundary conditions [49], the relative displacement of an antivortex with respect to a vortex is analyzed in Fig. 4(b), which is named an infinite chain (pink circles). The period was chosen to match the width of the cross-ties from the structure in Fig. 4(a) resulting in a quasi-infinite repetition of the cross-tie structure. In contrast, the finite chain (green circles) shows the difference coordinate (antivortex minus vortex) from Fig. 4(a). Both curves stand in excellent agreement, indicating that the periodic antivortex-vortex chain is able to describe the relative displacement between vortices and antivortices quite well [50]. The boundary conditions can be represented by a rectangular microstructure as shown in Fig. 4(c). The dimensions of this rectangle are defined by the microstructure in Fig. 4(a), after cutting the four cross-ties in the center away and joining both end domains. The resulting structure is nearly a square. The red circles in Fig. 4(c) indicate the vortex core displacement in this rectangle. The simulated curve stands in excellent agreement with the vortex core positions from Fig. 4(a), which verifies that the vortex position in Fig. 4(a) is defined solely by the boundary domains of the microstructure. As the distance between vortices and antivortices is fixed by coupling potential and Zeeman energy, the position of the antivortices is then defined relative to the vortex position. The shadowed curve shows again the experimental vortex displacement from Fig. 2(c).

Thus, the oppositely phased displacement of the antivortices to the vortex can be reduced to a vortex-antivortex combination with periodic boundary conditions, as shown in the inset of Fig. 4(b). This insulated relative or oppositely phased displacement reflects the coupling between both quasiparticles. Figure 5 displays the exchange (green), stray-field (blue), and Zeeman energy (red) for the single periodic structure in an external field, as obtained from simulation. In an external field the microstructure decreases its energy by displacing the quasiparticles relative to each other. This results in a net magnetic moment that reduces the Zeeman energy and therefore the total energy. This effect is counterbalanced by an increase of stray-field energy, leading to a well-defined equilibrium distance between both particles, as shown in Fig. 4(b). The increase of stray-field energy originates from magnetic charges that arise due to the deformation of the intermediate domains between vortices and antivortices. This results in a linear restoring force which is in analogy to a harmonic oscillator. The total energy (sum of

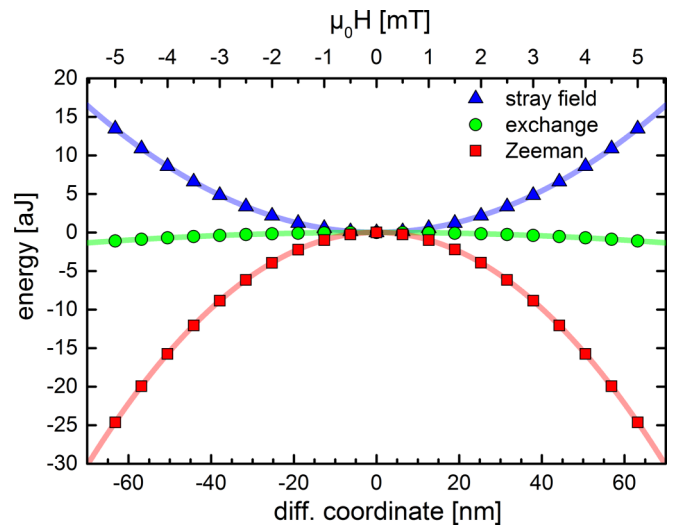


FIG. 5. Simulated energy contributions in a periodic vortex-antivortex-chain. The stray field (blue), exchange (green), and Zeeman (red) energy are plotted as a function of the external magnetic field (top axis) and a relative vortex-antivortex difference coordinate (bottom axis).

Zeeman, stray-field, and exchange energies) can therefore be written as

$$E = \frac{\kappa_{st} + \kappa_{ex}}{2} \cdot \Delta x^2 + D_Z \cdot \Delta x \cdot \mu_0 H,$$

where κ_{st} and κ_{ex} are the force constants due to the stray-field and the exchange energy, respectively, and D_Z denotes the strength of the Zeeman energy. A fit yields $\kappa_{st} = (6.73 \pm 0.01) \times 10^{-3} \frac{\text{J}}{\text{m}^2}$, $\kappa_{ex} = -(0.55 \pm 0.01) \times 10^{-3} \frac{\text{J}}{\text{m}^2}$, and $D_Z = -(7.79 \pm 0.01) \times 10^{-8} \frac{\text{J}}{\text{Tm}}$. The total spring constant, mainly due to the stray-field energy, is only slightly lowered by the exchange energy. Furthermore, the excellent agreement between finite and infinite vortex-antivortex chain in Fig. 4(b) shows that only next-neighbor coupling between vortices and antivortices must be considered. The deviations from this ansatz are visible in Fig. 4(a), as the individual (anti-)vortices have slightly different amplitudes due to a different number of neighbors. As this effect is small, it is beyond visibility in the experiment and supports the claim that only next-neighbor coupling has to be accounted for.

IV. CONCLUSION

The coupling between vortices and antivortices in FeCoSiB microstructures was studied experimentally by TR-SEMPA. In a vortex-antivortex chain, the quasiparticles oscillate at opposite phase to each other (in analogy to an optical mode) under external field drive. An additional common motion occurs (in analogy to an acoustic mode), leading in total to a stronger field-dependent displacement for the vortices compared to the antivortices. Micromagnetic simulations are in excellent agreement with the experimental findings and show that common and relative displacements can be described by two reduced microstructures. The boundary condition is described by a rectangular microstructure containing only one

vortex and defines the position of the vortices in the finite chain. The relative displacement between vortices and antivortices can be reproduced in an infinite, periodic vortex-antivortex chain, where the antivortices are solely coupled to the vortex positions.

ACKNOWLEDGMENTS

The work was supported by DFG within Grant No. SFB668. We gratefully acknowledge support of Volker Rößisch, Dr. Dirk Meyners, and Professor Dr. Eckard Quand from Kiel University for preparing the FeCoSiB films.

-
- [1] A. Hubert and R. Schäfer, *Magnetic Domains: The Analysis of Magnetic Microstructures* (Springer, Berlin, 2009).
- [2] E. Feldtkeller and H. Thomas, *Phys. Kondens. Mater.* **4**, 8 (1965).
- [3] E. E. Huber, D. O. Smith, and J. B. Goodenough, *J. Appl. Phys.* **29**, 294 (1958).
- [4] J. Raabe, R. Pulwey, R. Sattler, T. Schweinbock, J. Zweck, and D. Weiss, *J. Appl. Phys.* **88**, 4437 (2000).
- [5] T. Shinjo, T. Okuno, R. Hassdorf, K. Shigeto, and T. Ono, *Science* **289**, 930 (2000).
- [6] A. Wachowiak, J. Wiebe, M. Bode, O. Pietzsch, M. Morgenstern, and R. Wiesendanger, *Science* **298**, 577 (2002).
- [7] A. A. Thiele, *J. Appl. Phys.* **45**, 377 (1974).
- [8] S.-B. Choe, Y. Acremann, A. Scholl, A. Bauer, A. Doran, J. Stöhr, and H. A. Padmore, *Science* **304**, 420 (2004).
- [9] K. W. Chou, A. Puzic, H. Stoll, D. Dolgos, G. Schutz, B. Van Waeyenberge, A. Vansteenkiste, T. Tylliszczak, G. Woltersdorf, and C. H. Back, *Appl. Phys. Lett.* **90**, 202505 (2007).
- [10] K. Y. Guslienko, B. A. Ivanov, V. Novosad, Y. Otani, H. Shima, and K. Fukamichi, *J. Appl. Phys.* **91**, 8037 (2002).
- [11] K. Y. Guslienko, X. F. Han, D. J. Keavney, R. Divan, and S. D. Bader, *Phys. Rev. Lett.* **96**, 067205 (2006).
- [12] H. H. Langner, L. Bocklage, T. Matsuyama, and G. Meier, *Phys. Rev. B* **87**, 064420 (2013).
- [13] V. Novosad, F. Y. Fradin, P. E. Roy, K. S. Buchanan, K. Y. Guslienko, and S. D. Bader, *Phys. Rev. B* **72**, 024455 (2005).
- [14] V. S. Pribiag, I. N. Krivorotov, G. D. Fuchs, P. M. Braganca, O. Ozatay, J. C. Sankey, D. C. Ralph, and R. A. Buhrman, *Nat. Phys.* **3**, 498 (2007).
- [15] S. Rößler, S. Hankemeier, B. Krüger, F. Balhorn, R. Frömter, and H. P. Oepen, *Phys. Rev. B* **89**, 174426 (2014).
- [16] J. Shibata, Y. Nakatani, G. Tatara, H. Kohno, and Y. Otani, *Phys. Rev. B* **73**, 020403 (2006).
- [17] M. Pues, M. Martens, and G. Meier, *J. Appl. Phys.* **116**, 153903 (2014).
- [18] K. Shigeto, T. Okuno, K. Mibu, T. Shinjo, and T. Ono, *Appl. Phys. Lett.* **80**, 4190 (2002).
- [19] K. Y. Guslienko, V. Novosad, Y. Otani, H. Shima, and K. Fukamichi, *Appl. Phys. Lett.* **78**, 3848 (2001).
- [20] B. Krüger, A. Drews, M. Bolte, U. Merkt, D. Pfannkuche, and G. Meier, *Phys. Rev. B* **76**, 224426 (2007).
- [21] B. Krüger, M. Najafi, S. Bohlens, R. Frömter, D. P. F. Möller, and D. Pfannkuche, *Phys. Rev. Lett.* **104**, 077201 (2010).
- [22] B. Krüger, A. Drews, M. Bolte, U. Merkt, D. Pfannkuche, and G. Meier, *J. Appl. Phys.* **103**, 07A501 (2008).
- [23] T. Eggebrecht, M. Möller, J. G. Gatzmann, N. Rubiano da Silva, A. Feist, U. Martens, H. Ulrichs, M. Münzenberg, C. Ropers, and S. Schäfer, *Phys. Rev. Lett.* **118**, 097203 (2017).
- [24] H. Hata, M. Goto, A. Yamaguchi, T. Sato, Y. Nakatani, and Y. Nozaki, *Phys. Rev. B* **90**, 104418 (2014).
- [25] J. Shibata, K. Shigeto, and Y. Otani, *Phys. Rev. B* **67**, 224404 (2003).
- [26] O. V. Sukhostavets, J. M. Gonzalez, and K. Y. Guslienko, *Appl. Phys. Express* **4**, 065003 (2011).
- [27] S. Jain, H. Schultheiss, O. Heinonen, F. Y. Fradin, J. E. Pearson, S. D. Bader, and V. Novosad, *Phys. Rev. B* **86**, 214418 (2012).
- [28] H. Jung, K.-S. Lee, D.-E. Jeong, Y.-S. Choi, Y.-S. Yu, D.-S. Han, A. Vogel, L. Bocklage, G. Meier, M.-Y. Im, P. Fischer, and S.-K. Kim, *Sci. Rep.* **1**, 59 (2011).
- [29] J. Miguel, J. Sánchez-Barriga, D. Bayer, J. Kurde, B. Heitkamp, M. Piantek, F. Kronast, M. Aeschlimann, H. A. Dürr, and W. Kuch, *J. Phys.: Condens. Matter* **21**, 496001 (2009).
- [30] R. Frömter, F. Kloodt, S. Rößler, A. Frauen, P. Staeck, D. R. Cavicchia, L. Bocklage, V. Rößisch, E. Quandt, and H. P. Oepen, *Appl. Phys. Lett.* **108**, 142401 (2016).
- [31] K. Koike and K. Hayakawa, *Jpn. J. Appl. Phys.* **23**, L187 (1984).
- [32] H. P. Oepen and J. Kirschner, *J. Phys., Colloq.* **49**, 1853 (1988).
- [33] J. Unguris, D. T. Pierce, and R. J. Celotta, *Rev. Sci. Instrum.* **57**, 1314 (1986).
- [34] R. Frömter, S. Hankemeier, H. P. Oepen, and J. Kirschner, *Rev. Sci. Instrum.* **82**, 033704 (2011).
- [35] H. Hopster and H. P. Oepen, in *SEMPA Studies of Thin Films, Structures, and Exchange Coupled Layers. Magnetic Microscopy of Nanostructures* (Springer, Berlin, 2005), p. 137.
- [36] H. P. Oepen and R. Frömter, *Scanning Electron Microscopy with Polarisation Analysis. Handbook of Magnetism and Advanced Magnetic Materials* (Wiley, Chichester, UK, 2007).
- [37] F. Lofink, A. Philippi-Kobs, M. R. Rahbar Azad, S. Hankemeier, G. Hoffmann, R. Frömter, and H. P. Oepen, *Phys. Rev. Appl.* **8**, 024008 (2017).
- [38] K. Koike, *Microscopy* **62**, 177 (2013).
- [39] B. Boehm, A. Bisig, A. Bischof, G. Stefanou, B. J. Hickey, and R. Allenspach, *Phys. Rev. B* **95**, 180406 (2017).
- [40] E. C. Corredor, S. Kuhrau, F. Kloodt-Twesten, R. Frömter, and H. P. Oepen, *Phys. Rev. B* **96**, 060410(R) (2017).
- [41] J. Lucassen, F. Kloodt-Twesten, R. Frömter, H. P. Oepen, R. A. Duine, H. J. Swagten, B. Koopmans, and R. Lavrijsen, *Appl. Phys. Lett.* **111**, 132403 (2017).
- [42] Y. Acremann, V. Chembrolu, J. P. Strachan, T. Tylliszczak, and J. Stöhr, *Rev. Sci. Instrum.* **78**, 014702 (2007).
- [43] N. Rubiano da Silva, M. Möller, A. Feist, H. Ulrichs, C. Ropers, and S. Schäfer, [arXiv:1710.03307](https://arxiv.org/abs/1710.03307).
- [44] K. Kuepper, M. Buess, J. Raabe, C. Quitmann, and J. Fassbender, *Phys. Rev. Lett.* **99**, 167202 (2007).
- [45] The Oersted field is numerically calculated under the assumption of a homogeneous current over the rectangular cross-section of the microstrip.
- [46] Fe₇₀Co₈Si₁₂B₁₀ consists mainly of Fe. Therefore, the exchange constant of Fe (22 pJ/m) [51] is used for the micromagnetic simulations. The exchange constant of Co is slightly higher (31 pJ/m) [51].
- [47] B. Mozooni and J. McCord, *Appl. Phys. Lett.* **107**, 042402 (2015).

- [48] C. Abert, A. Drews, B. Krüger, and G. Selke, MICROMAGNUM, v0.2 (2016), <http://micromagnum.informatik.uni-hamburg.de/>.
- [49] By periodic boundary conditions we signify that for calculating the stray field the simulated structure is repeated 200 times in the x direction. The simulations were reproduced with 500 repeats to rule out that the amount of repeats is affecting the result.
- [50] Under the action of an external field the coupling potential defines only the difference coordinate between vortex and antivortex in the periodic structure. Although the system is translation invariant, both particles follow well-defined trajectories, given by the Thiele equation, that depend on the starting position of both quasiparticles, their gyrovector (same absolute value for both), and their dissipation tensor (different for both). As the dissipation for the antivortex is larger, its absolute movement is smaller. In contrast to the finite structure no restoring force positions both particles in the translation-invariant system. In any case vortex and antivortex move in opposite directions, showing clearly that an explanation of the experimentally found slopes with different dissipation tensors is not possible.
- [51] H. Kronmüller and M. Fähnle, *Micromagnetism and the Microstructure of Ferromagnetic Solids* (Cambridge University Press, Cambridge, England, 2009).